ADVANCED ENERGY MATERIALS

Sn-Alloy Foil Electrode with Mechanical Prelithiation: Full-Cell Performance up to 200 Cycles

Hui Xu, Sa Li,* Xinlong Chen, Can Zhang, Wenjian Liu, Huimin Fan, Yue Yu, Yunhui Huang,* and Ju Li*

Self-supporting Sn foil is a promising high-volumetric-capacity anode for lithium ion batteries (LIBs), but it suffers from low initial Coulombic efficiency (ICE). Here, mechanical prelithiation is adopted to improve ICE, and it is found that Sn foils with coarser grains are prone to cause electrode damage. To mitigate damage and prepare thinner lithiated electrodes, 3Ag0.5Cu96.5Sn foil is used that has more refined grains (5–10 µm) instead of Sn (50–100 µm), where the abundant grain boundaries (GBs) offer more sliding systems to release stress and reduce deep fractures. Thus, the thickness of Li$_x$3Ag0.5Cu96.5Sn can be reduced to 50 µm, compared to 100 µm Li$_x$Sn. When the foils contact open air, the Sn-Li-O(H) products are more stable than Li-O(H), thus Li$_x$3Ag0.5Cu96.5Sn shows outstanding air stability. The as-prepared 50 µm foil anode achieves stable 200 cycles in LiFePO$_4$//Li$_x$3Ag0.5Cu96.5Sn full cell (≈2.65 mAh cm^{-2}) and the capacity retention is 95%. Even at 5C, the capacity of Li$_x$3Ag0.5Cu96.5Sn is still up to ≈1.8 mAh cm^{-2}. The cycle life of NCM523//Li$_x$3Ag0.5Cu96.5Sn full cell exceeds that of NCM523//Li. Furthermore, 70 µm Li$_x$3Ag0.5Cu96.5Sn is used as double-sided anode for a 3 cm × 2.8 cm pouch cell and its actual volumetric capacity density is 674 mAh cm^{-3} after 50 cycles.

1. Introduction

Self-supporting tin foil should be an attractive anode for lithium ion batteries considering its high theoretical capacity in Sn↔Li$_x$Sn alloying reaction (990 mAh g^{-1} or 1990.6 mAh cm^{-3} for Li$_{4.4}$Sn),[1,2] metallurgical processability (easily rolled down

H. Xu, Dr. S. Li, X. Chen, C. Zhang, W. Liu, H. Fan, Y. Yu, Prof. Y. Huang
School of Materials Science and Engineering
Tongji University
Shanghai 201804, China
E-mail: lisa@tongji.edu.cn; huangyh@tongji.edu.cn
H. Xu, Dr. S. Li, X. Chen, C. Zhang, W. Liu, H. Fan, Y. Yu, Prof. Y. Huang
Institute of New Energy for Vehicles
Tongji University
Shanghai 201804, China
Prof. J. Li
Department of Nuclear Science and Engineering and Department of Materials Science and Engineering
Massachusetts Institute of Technology
Cambridge, MA 02139, USA
E-mail: liju@mit.edu

to tens of micrometers thickness), excellent electrical conductivity, and initially high density (7.28 g cm^{-3}). But curiously, metallic foil anodes are rarely reported in the literature, except for the pure Li metal foil. Most reports about Sn↔Li$_x$Sn based anode focused on nanoparticles of Sn or SnO$_2$. In the few works on Sn foil or Sn-based thin film prepared by costly electron-beam deposition or magnetron sputtering, the performance seems not attractive. For example, 15 µm pure tin foil electrode reported by Yang et al.[3] in 2003 showed a rapid capacity decay just after ten deep cycles and then the electrode had pulverized to black mud-like materials. In addition to mechanical failure caused by pulverization, the extremely low initial Coulombic efficiency (ICE) of metallic foil anode is another tough problem. Theoretically, since the initial surface area of dense tin foil is far smaller than that of tin nanoparticles (>10^3× initial contact area with the electrolyte), the electrolyte decomposition is supposed to be greatly reduced and thus ICE is expected to be better.[4–6] However, the actual results are perplexing. In 2005, Hu et al.[7] had showed that ICE of Sn-Cu thin film anode prepared by electron-beam evaporation deposition was 84%, which is similar to that of nano-architectured Sn anodes,[8,9] while the ICE of annealed Sn-Cu thin film that has a more compact structure and larger grains was actually 30%, opposite to what one might have expected.[7,10,11] Similar result that the ICE of dense Sn foil is surprisingly low to 10% to 20% also was found in our previous work[12] and Figure S1 in the Supporting Information. We had explored the reason in previous work and found the low ICE is caused by the serious foil pulverization and obvious catalytic effect of Sn metal on the decomposition of electrolyte.[12]

In practical full cells, to cope with the cyclable lithium loss, anode prelithiation is necessary.[13] Common prelithiation methods such as electrical shorting and chemical routes[14–17] could create excess inventory to prepare for the future loss of cyclable lithium, but the prelithiation process is usually complex and has difficulty scaling up industrially. Pure Li metal can react with Sn through direct contact. Taking advantage of this, we designed a facile mechanical prelithiation method, which does not require organic electrolyte or expensive equipment, where the reaction time is sped up by
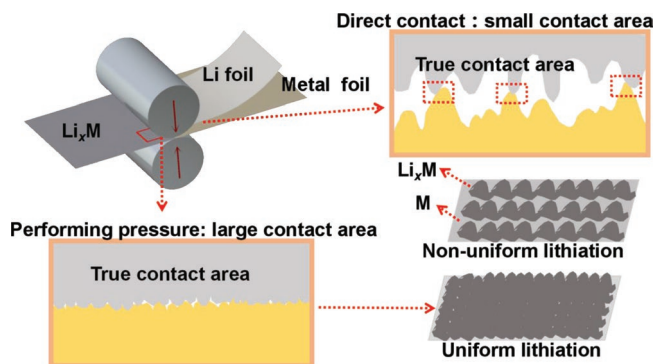
Figure 1. Schematic diagram of mechanical prelithiation method.

applying mechanical pressure in rolling, to increase the true contact area between the two reacting metals. The schematic diagram is presented in **Figure 1**, typically, Sn and Li foils are physically stacked together and pressed by a roller, herein, the soft lithium-metal (body-centered cubic or BCC phase) will creep at room temperature, since one is already at 2/3 of Li_{BCC}'s absolute melting temperature ($T/T_M = 0.66$), and diffusion transport can support a Newtonian fluid like viscous creep motion with an effective polycrystalline viscosity.[18] The Li_{BCC} phase becomes "fluid-like"[18] under mechanical pressure and thus the true contact area between Sn and Li foils is largely increased, greatly accelerating the prelithiation and also making the degree of prelithiation more homogeneous. After prelithiation, the ICE of LiFePO$_4$(LFP)//Li$_x$Sn full cell was improved to 94% from 20% and the full cell can deeply cycle 200 times at ≈2.65 mAh cm^{-2}.[12] However, it is worth mentioning that in that previous work the thickness of Li$_x$Sn was ≈100 μm, 25% thicker than the commercial graphite anode of the same areal capacity (≈80 μm thick including copper current collector).[19] Generally speaking, regardless of electrochemical or mechanical lithiation, we find that the thinner the foil, the less damage tolerant it becomes in subsequent electrochemical cycling. The drive toward thinner free-standing foil electrode for higher volumetric energy density full cells behooves us to unveil its underlying damage mechanism and find a solution to improve the "lithiation/delithiation ductility" (LDD). In this paper, we defined the term of "lithiation/delithiation ductility" (LDD) as the ability of a host material to deform and maintain electronic percolation without catastrophic failure and electrode damage due to electrochemical reactions induced volume expansion/ shrinkage and shape change.

Interestingly, postmortem examination of electrochemically lithiated pure Sn foil reveals three typical features, including millimeter-scale mountain range-like undulations (**Figure 2**a and Figure S2a,b, Supporting Information), 10 μm scale gully cracks, and loose fragmental debris as small as few hundred nanometers and as large as ≈10 μm (Figure 2b,c and Figure S3ab, Supporting Information). In contrast, the surface of mechanically prelithiated pure Sn foil is quite flat (Figure 2d) and the millimeter-scale undulations in Figure 2a is suppressed because of the externally applied compressive stress. However, further analysis finds the electrode still has serious damage, such as, 10 μm scale cracks (Figure 2e) and structural decrepitation (Figure 2f) which are factors that

hinder further thinning of Li$_x$Sn foil by rolling. (In rolling of metal sheets, it is well known that rolling cracks can form, and lithiation will further reduce the amount one can thin down the sheet before gross mechanical/electrical failures.) After careful analysis and comparison, we find the lithiation process of foil-like electrode is quite similar to tectonic geomorphology.[20,21] We illustrate the microstructural evolutions during Sn foil prelithiation in Figure 2g.

During initial stages of lithiating, the alloying reaction of Sn + xLi → Li$_x$Sn would firstly occur at the lithium-wetting surface,[22] followed by lithiation along GBs because of the rapid Li$^+$ diffusion, inducing expansion and strain concentration there.[23,24] Note that the GBs are subjected to stress in the cell during lithiation, making GB sliding the main mechanism for accommodating inelastic deformation and stress relaxation.[24–26] However, if the internal residual stress fails to be released well due to inadequate GB sliding, for example in the coarse-grained Sn foil where the GBs are limited, some gully-like opening fractures would be created and propagate readily, exposing fresh surfaces that allow infiltration of liquid electrolyte from above. Moreover, similar to geomorphic process, where the surface relief leads to an uneven distribution of water, such a foil electrode with different scales of cracks would cause liquid electrolyte localization and subsequent non-uniform electrochemical reaction.

Since GBs facilitate stress relief and thus alleviate aforementioned mechanical damage, it is reasonable to assume that grain size refinement might be an effective strategy to achieve more uniform prelithiation and thinner prelithiated foil without gross failure, i.e., better LDD. Therefore, adding in few percent of other elements, which is a classic metallurgical approach for grain refinement, should be beneficial.[27,28] As welding solders, there are commercialized tin-based alloys on the market.[29–31] In this work, 3Ag0.5Cu96.5Sn alloy (i.e., 3 wt% Ag, 0.5 wt% Cu, 96.5 wt% Sn) was purchased and rolled down to sheet. In contrast to pure Sn foil with an average grain size of ≈50–100 μm, its grain size is ≈5–10 μm, because a small amount of silver and copper based precipitates stops grain growth by the Zener pinning of GBs. In contrast to pure Sn foil that comes apart immediately after prelithiation, decent mechanical strength was achieved in lithiated 3Ag0.5Cu96.5Sn foil rolled down to 50 μm thickness, which should be attributed to densified GB sliding systems that enhance relaxation of internal stress. In this regard, we believe LDD is quite different from mechanical ductility: that is, with decreasing grain size D, mechanical ductility usually decreases together with Hall-Petch hardening, but LDD actually increases, due to the different roles GBs play in mechanical deformation (as obstacles to dislocation motion) versus phase transformation based LDD (GB sliding as the main stress relief mechanism). Simultaneously, benefiting from mechanical prelithiation, Li$^+$ diffusion as well as the Faraday impedance and electrode wettability were improved. The as-prepared 50 μm thick foil anode has achieved an impressive stable 200 cycles and the capacity retention was up 95% in LFP//Li$_x$3Ag0.5Cu96.5Sn full cells using the common LiPF$_6$-in-carbonates liquid electrolyte. Even with a high charging/discharging rate of 5C, the areal capacity of Li$_x$3Ag0.5Cu96.5Sn is still up to ≈1.8 mAh cm^{-2}.
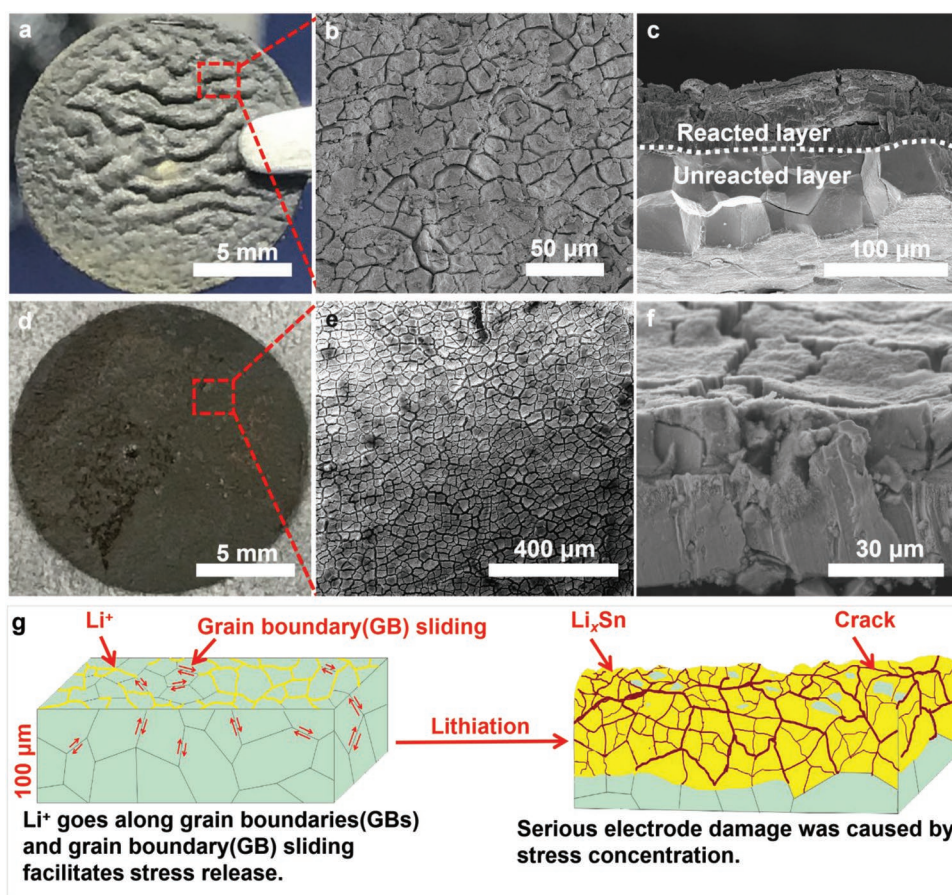
Figure 2. Exploring lithiation process of Sn foil based on electrochemical and mechanical methods. a) Visual millimeter-scale mountain range-like undulations after electrochemical lithiation. b,c) SEM images of 10 µm scale gully cracks and loose fragmental debris after electrochemical lithiation. d) Digital photo of prelithiated Sn foil by the mechanical method. The foil surface is flat and the rugged mountain-like undulations is eliminated by applied pressure. e,f) SEM images of gully cracks and loose fragmental debris after mechanical prelithiation. f) The electrode shows serious damage and even structural decrepitation. g) Proposed lithiation process of Sn foil-like electrode.

Besides, the cycle stability of LiNi$_{0.5}$Co$_{0.2}$Mn$_{0.3}$O$_2$(NCM523)// Li$_x$3Ag0.5Cu96.5Sn full cell is obviously superior to that of NCM523//Li metal cell. Finally, we demonstrate a 70 µm thick prelithiated Li$_x$3Ag0.5Cu96.5Sn foil that serves as double-sided anode in a 3 cm × 2.8 cm pouch cell, can achieve a highly respectable volumetric capacity density of 674 mAh cm^{-3}.

2. Results and Discussion

In this study, commercially available 3Ag0.5Cu96.5Sn alloy was employed directly as the starting material instead of pure Sn foil. Compared to pure Sn that has an average ≈50–100 µm grain size (**Figure 3**a and Figure S4, Supporting Information), the grain size of 3Ag0.5Cu96.5Sn has become so small that optical microscope cannot clearly identify it (Figure 3b and Figure S5, Supporting Information). However, from the cross-sectional scanning electron microscope (SEM) image of 3Ag0.5Cu96.5Sn in Figure 3c, we can distinguish the tightly packed 5–10 µm grains, which is just about one tenth of that of pure Sn. This is because the Ag and Cu

based precipitates stop grain growth by Zener pinning of GB during the casting. The equilibrium phase diagram shows there are Ag$_3$Sn and Cu$_6$Sn$_5$ phases in 3Ag0.5Cu96.5Sn foil[27] (Figures S6 and S7, Supporting Information), but it cannot tell us the distribution and particle size. Thus, transmission electron microscope (TEM) and SEM characterizations were conducted,[7,32] and some ≈200 nm Ag$_3$Sn particles scattered in foil matrix were evidently observed (Figure 3d,e and Figure S8, Supporting Information). On the other hand, Cu element is involved in two kinds of solid solutions, Cu-Sn and Ag-Cu-Sn (Figure 3f,g) instead of Cu$_6$Sn$_5$ phase,[33,34] which may be caused by a rapid cooling during processing. X-ray diffraction (XRD) result also confirmed this, only peaks of Ag$_3$Sn (indicated with the pink) and Sn (the orange) were detected but no Cu$_6$Sn$_5$ peaks in Figure 3h. The tensile strength, reflecting ability of resistance to mechanical deformation,[29,35,36] also was enhanced to 50 MPa from 13 MPa of pure Sn (Figure 3i).

We start with a 3Ag0.5Cu96.5Sn foil to prepare thinner prelithiated foil electrode by the mechanical prelithiation method in Figure 1, where a 45 µm × 10 cm × 3.5 cm 3Ag0.5Cu96.5Sn foil (inset of **Figure 4**a) and a 25 µm × 10 cm × 3.5 cm Li foil
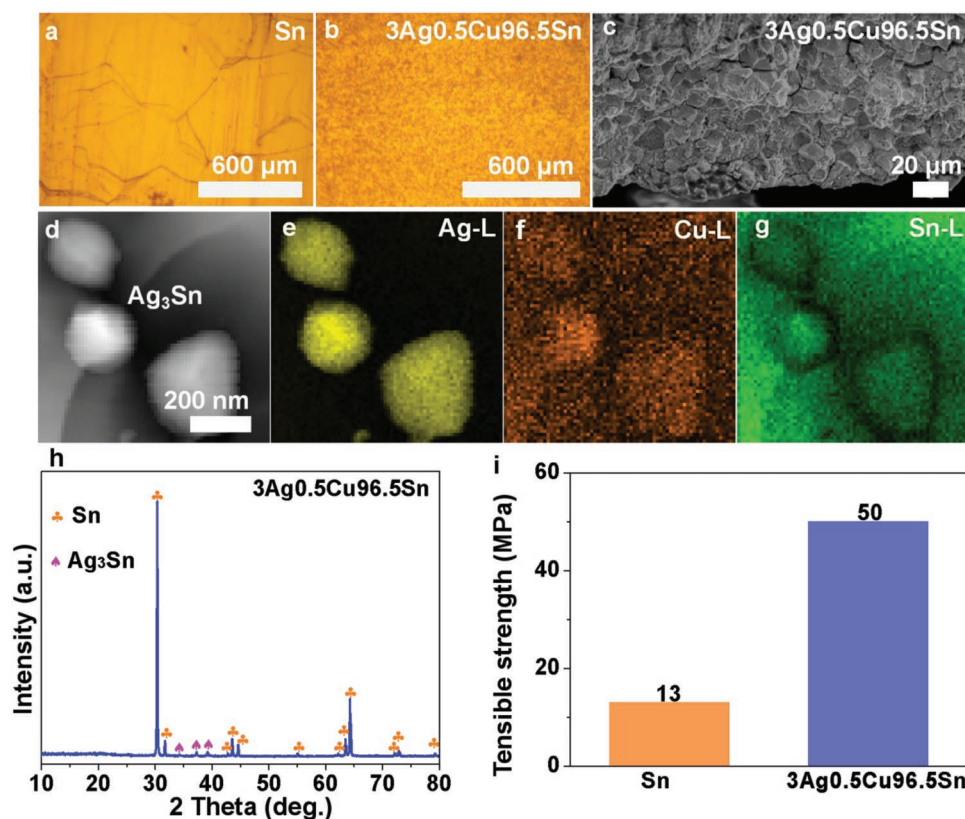
Figure 3. Characterization of Sn and 3Ag0.5Cu96.5Sn foils. Optical images of a) etched pure Sn foil and b) etched 3Ag0.5Cu96.5Sn foil. c) Sn grains of 3Ag0.5Cu96.5Sn observation by the cross-sectional SEM image of 3Ag0.5Cu96.5Sn foil. d) TEM characterization of 3Ag0.5Cu96.5Sn alloy foil. And ≈200 nm Ag_3Sn particles were determined. Distribution of e) Ag element, f) Cu element, and g) Sn element in 3Ag0.5Cu96.5Sn alloy foil. h) XRD analysis of 3Ag0.5Cu96.5Sn foil. The Ag_3Sn (the pink) and Sn (the orange) were determined. i) The tensile strength of Sn foil (the orange) and 3Ag0.5Cu96.5Sn foil (the blue).

were stacked, and pressed together by a roller at 30 MPa pressure. The operation and the influence of pressure on lithiation degree had been explored in our previous work.[12] The Li metal spreads like butter on the 3Ag0.5Cu96.5Sn, which is itself also extending. The alloying and bonding reaction (mechanical prelithiation) occurs simultaneously with the mechanical deformation of the remaining Li_{BCC} and 3Ag0.5Cu96.5Sn phases, until they become one dense layer of 50 μm × 18 cm × 4.5 cm sized Li_x3Ag0.5Cu96.5Sn foil, which is mechanically stable (no huge rolling cracks and can be handled easily without failure) and electronically percolating. The visual image of the as-formed foil was shown in Figure 4a, the previous silver-white foil (inset of Figure 4a) becomes dark after prelithiation. The density of micro cracks of Li_x3Ag0.5Cu96.5Sn (Figure 4b) is obviously less than that of pure Sn (Figure 2e) due to abundant GB slippage to relieve phase-transformation induced stress. The cross-sectional SEM of Li_x3Ag0.5Cu96.5Sn also shows a more stable morphology (Figure 4c) instead of the smashed and decrepitated fragments as found in Li_xSn foil. The phase composition of the Li_x3Ag0.5Cu96.5Sn foil was then examined by XRD in Figure 4d, where only peaks of crystalized $Li_{13}Sn_5$ were found. Even though we cannot identify Ag-related and Cu-related phases from the XRD peaks, Yin et al.[37] and Hu et al.[7] showed Ag and Cu elements may form lithium-containing mesophase, e.g., $LiAg_2Sn$, Li_2AgSn, Li_2Ag and

Li_3CuSn. We also determined the electrochemically retrievable lithium inventory of Li_xSn and Li_x3Ag0.5Cu96.5Sn, as shown in Figure 4e, which is ≈3 mAh cm⁻² and ≈3.2 mAh cm⁻², respectively. It should be noted that because the Li_{BCC} becomes "fluid-like" and spreads out on the surface of Sn foil under mechanical pressure, the actual lithium alloyed by Sn is less than 25 μm and therefore the corresponding lithium inventory also is less than 5 mAh cm⁻².

In addition to the prestored lithium, lithium diffusivity and electrolyte wetting are largely improved as well after mechanical prelithiation. Because dense foil electrodes generally have long solid-state diffusion distance for lithiation/delithiation, even with grain boundary diffusivity up to four orders of magnitude larger than bulk diffusivity at room temperature,[38] the lithium conductivity is still poor. However, once intergranular opening was induced by huge volume and shape changes during prelithiation, as revealed in Figure 4b,c, the liquid electrolyte will seep into the cracks, replacing the originally Li(metallic) transport along GB by Li⁺(electrolyte) transport in the liquid electrolyte along the GB, boosting Li⁺ conductivity there. We demonstrate that Li transport in prelithiated foil was significantly faster by performing CV test of different scan rates on 3Ag0.5Cu96.5Sn (**Figure 5a**) and Li_x3Ag0.5Cu96.5Sn (Figure 5b) foil electrodes. The stronger Li-Sn alloy peaks at 0.6, 0.4 V (Figure 5b) indicate more favorable Li⁺ diffusion. We also roughly calculated the
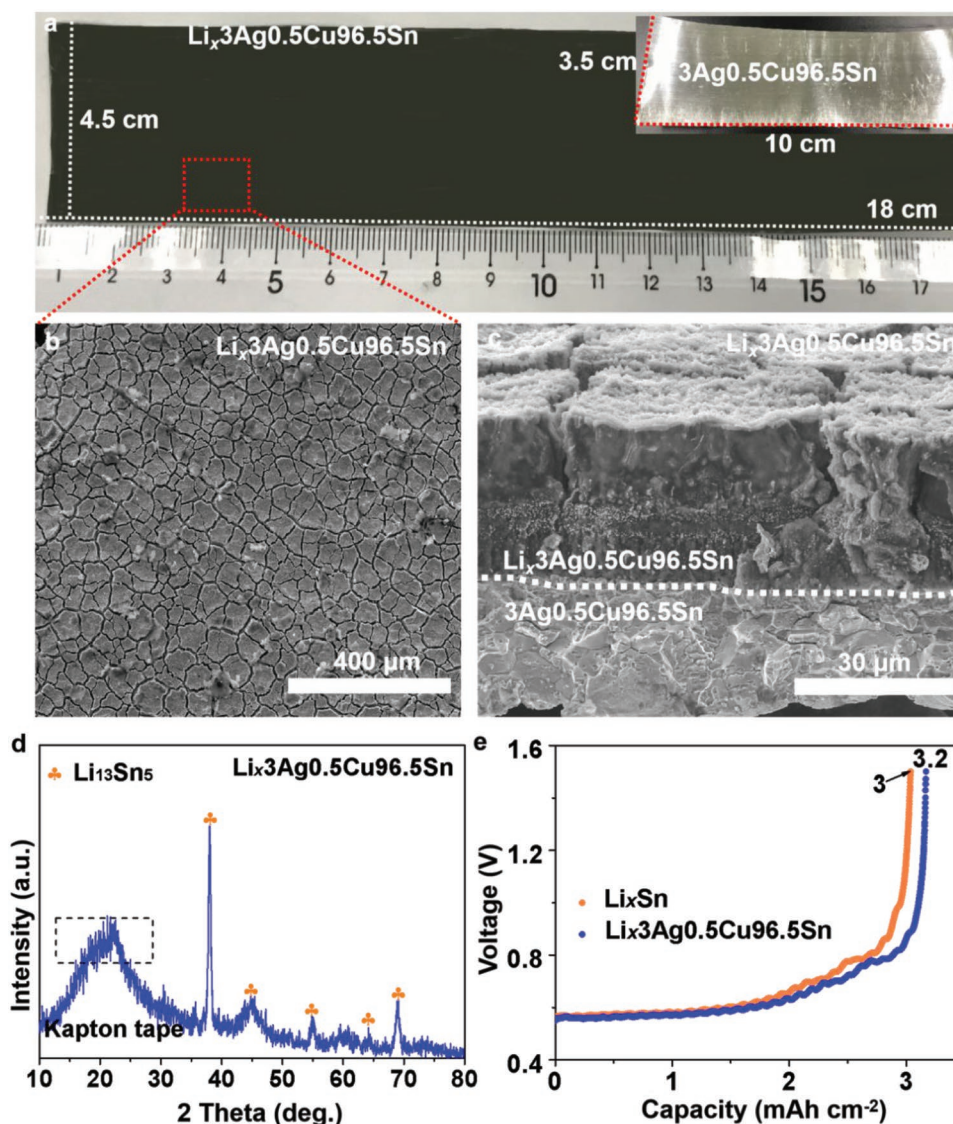
Figure 4. Preparation and characterization of Li$_x$3Ag0.5Cu96.5Sn foil. a) Visual image of Li$_x$3Ag0.5Cu96.5Sn foil. The inset is initial 3Ag0.5Cu96.5Sn alloy foil with metallic luster. b,c) SEM images of the fresh Li$_x$3Ag0.5Cu96.5Sn foil. d) XRD analysis of Li$_x$3Ag0.5Cu96.5Sn foil and only peaks of Li$_{13}$Sn$_5$ were determined. e) The lithium inventory of Li$_x$Sn (the orange) and Li$_x$3Ag0.5Cu96.5Sn foil (the blue) was determined by delithiating to 1.5 V.

diffusion coefficient based on the Randles-Sevcik relationship of peak current and CV sweep rate.[39,40]

$$I_\mathrm{p} = Kn^{3/2}AD^{1/2}v^{1/2}C \tag{1}$$

where I_p is the peak current (A), K is a constant of standard conditions (25 °C, $K = 2.69 \times 10^5$ C mol^{-1} V$^{-1/2}$), n is the number of electrons transferred per redox event (taken to be 1), A is the electroactive area (the diameter of electrode disc is 12 mm, the experiment result reveals the entire top ≈13 µm layer is involved in reaction. According to experimental measurement, the mass is about 10 mg, so the electroactive area of Sn foil electrode is 1.13×10^2 cm^2 g^{-1}), v is the CV scan rate (V s^{-1}), and C is the bulk concentration of lithium in electrode calculated from LiSn (0.0397 mol cm^{-3}). Note that the charge transfer at interface is ignored and the rate-limiting

process is lithium diffusion in electrode bulk. Li$^+$ diffusion coefficient (D_{Li^+}) at the reduction peak (lithiation at ≈0.6 V) of Li$_x$3Ag0.5Cu96.5Sn alloy is estimated to 1×10^{-13} cm^2 s^{-1} and that at oxidation peak (delithiation at ≈1.2 V) is 2.53×10^{-13} cm^2 s^{-1}. It is one order of magnitude larger than 3Ag0.5Cu96.5Sn foil, where D_{Li^+} at the reduction peak (lithiation at ≈0.6 V) is 0.45×10^{-14} cm^2 s^{-1} and that is 1.18×10^{-14} cm^2 s^{-1} at oxidation peak (delithiation at ≈1.2 V). The linear relationship between peak current and square root of scan rate shows in Figure 5c and Figures S9 and S10 in the Supporting Information, the larger slope of Li$_x$3Ag0.5Cu96.5Sn (the blue) shows the faster Li$^+$ diffusion. Furthermore, the Faraday impedance decreased to 75 Ω (the blue) from the initial 1500 Ω (the orange) in Figure 5d, which implies Li$^+$ diffusivity was largely improved. Besides, the contact angle between electrolyte and electrode decreased
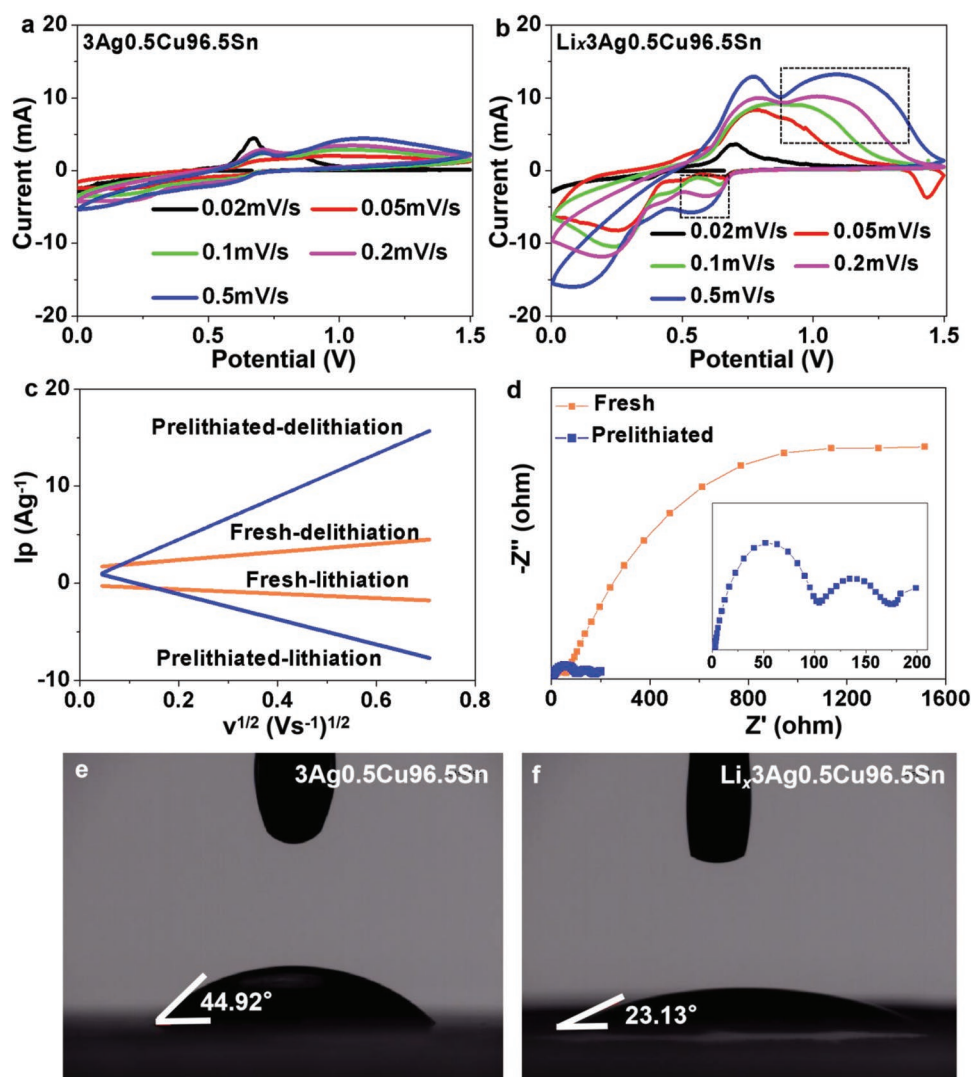
**ADVANCED
SCIENCE NEWS**

www.advancedsciencenews.com

**ADVANCED
ENERGY
MATERIALS**

www.advenergymat.de

Figure 5. Mechanical prelithiation improves lithium diffusivity and electrolyte wettability. CV tests of a) 3Ag0.5Cu96.5Sn and b) Li$_x$3Ag0.5Cu96.5Sn with different scan rates. c) The linear relationship between peak current and square root of scan rate. The orange is fresh foil (3Ag0.5Cu96.5Sn) and the blue is prelithiated foil (Li$_x$3Ag0.5Cu96.5Sn). d) EIS results of 3Ag0.5Cu96.5Sn foil (the orange) and Li$_x$3Ag0.5Cu96.5Sn foil (the blue). Contact angle test of electrolyte and e) 3Ag0.5Cu96.5Sn foil, f) Li$_x$3Ag0.5Cu96.5Sn foil.

to 23.13° from 44.92° (Figure 5e,f), indicating the better electrode wettability after prelithiation.

The air stability of a metallic foil electrode is extremely important for industrial battery assembly. Li metal foil, for example, needs to be carefully protected, and only very short exposure to ambient air with humidity can be allowed. For example, pure Li foil shows visible color change just after 5 s and becomes fully dark after 180 s (**Figure 6**a), so generally requires glove boxes, or at least dry room for battery assembly. Here, we examined the air stability by intentionally exposing Li$_x$3Ag0.5Cu96.5Sn electrode to ambient air for hours. As shown in Figure 6b, the fresh Li$_x$3Ag0.5Cu96.5Sn foil is black and electrochemically extractable lithium inventory is ≈2.98 mAh cm^{-2} (Figure 6c, the blue). After 12 h, there is no visually noticeable change and electrochemically extractable lithium inventory remains ≈2.96 mAh cm^{-2}, with almost no capacity decay (Figure 6c, the red). After exposure

to ambient air for 48 h, the foil surface became gray a little bit but the capacity retention is still ≈90% (see Figure 6c, the pink). After exposed for 72 h, the capacity retention still is 75% (see Figure 6c, the green), indicating surprisingly excellent air stability of prelithiated Sn foil. Note that the different delithiation plateaus in Figure 6c are because part of lithium was consumed in open air. The composition and constitution of phases in the matrix gradually change and some lithium-poor phases may even be produced, such as LiSn, resulting in the rising delithiation voltage plateaus.

When we characterize the Li$_x$3Ag0.5Cu96.5Sn foil exposed to air for 48 h by SEM, interestingly, the original cracks (Figure 4b) on Li$_x$3Ag0.5Cu96.5Sn foil surface seem to be cured and have disappeared mostly (Figure 6d), filled up by the passivating oxides. This negative feedback process of "caulking" the already-sparse microcracks (one crack every ≈50 µm in Figure 4c, compared to one crack every ≈10 µm in Figure 2b) to reduce

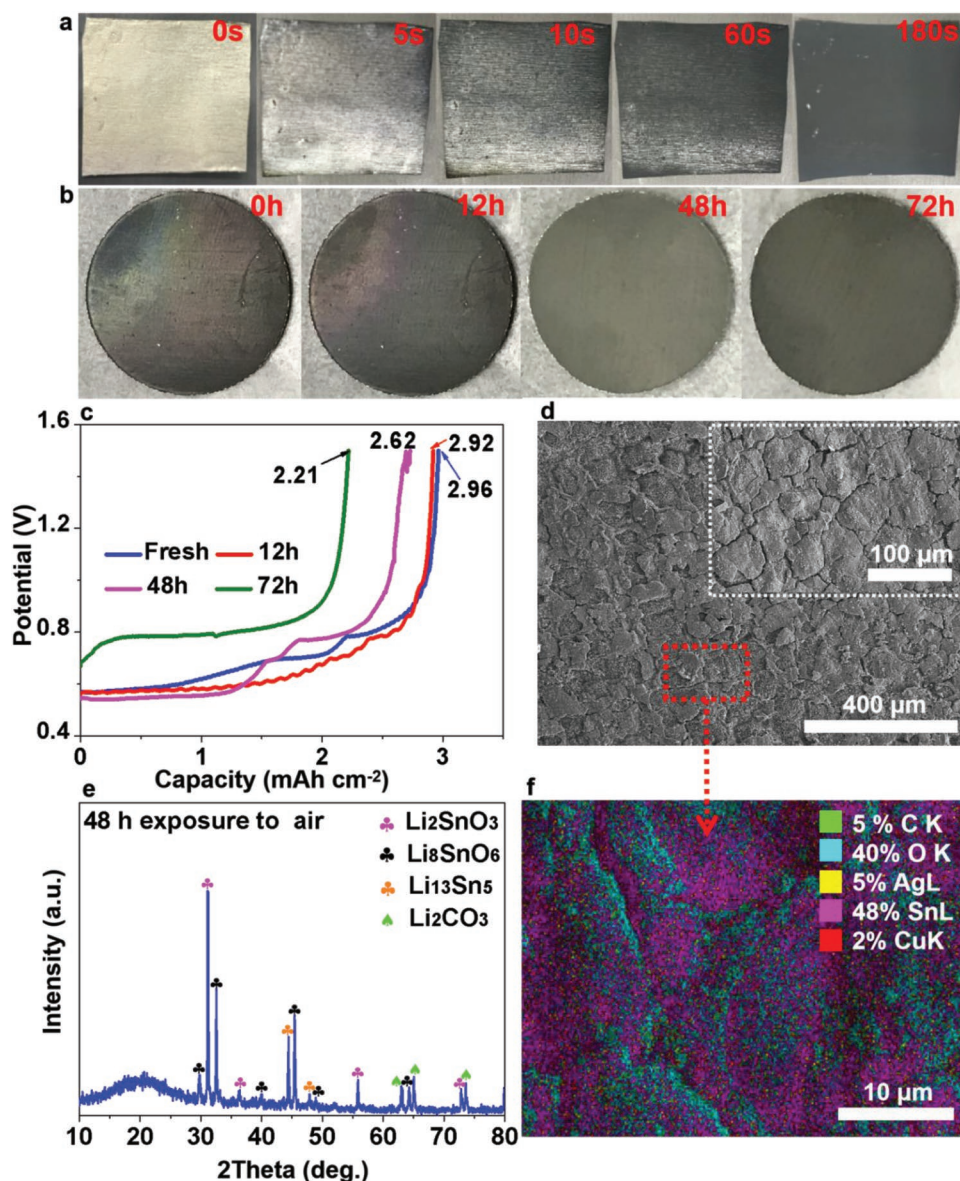**Figure 6.** The air stability analysis of Li$_x$3Ag0.5Cu96.5Sn foil electrode. a) The digital photos of pure Li foil exposed to air for different time. b) The digital photos of Li$_x$3Ag0.5Cu96.5Sn foil exposed to air for different hours. c) The lithium inventory of Li$_x$3Ag0.5Cu96.5Sn after different-hour exposure to air. d) SEM characterization of Li$_x$3Ag0.5Cu96.5Sn foil that was exposed to air for 48 h. e) XRD analysis of Li$_x$3Ag0.5Cu96.5Sn foil that was exposed to air for 48 h. f) EDS analysis of Li$_x$3Ag0.5Cu96.5Sn foil exposed to air for 48 h.

moisture infiltration underlies the superior air stability of our Li$_x$3Ag0.5Cu96.5Sn foil. Furthermore, we investigated the surface configuration after 48 h exposure in air to comprehensively understand the "self-healing" phenomenon. From XRD pattern in Figure 6e, a large amount of Li$_2$SnO$_3$ and Li$_8$SnO$_6$ as well as a little bit of Li$_2$CO$_3$ was identified in addition to initial Li$_{13}$Sn$_5$ phase. Besides, energy dispersive spectrometer (EDS) mapping in Figure 6f reveals the main elements on surface are Sn and O (lithium signal cannot be detected by EDS), also consistent with XRD result, implying Sn-Li-O(H) compounds were produced when exposing Li$_x$3Ag0.5Cu96.5Sn electrode to air. We speculate the generation of the denser Li-Sn-O(H) products is responsible for the self-repairing and eventually lead to the excellent air stability.

In order to determine the specific capacity of Li$_x$3Ag0.5Cu96.5Sn electrode, we punched a disc with a diameter of 8 mm (11.68 mg in weight) and paired it with lithium metal. The Li$_x$3Ag0.5Cu96.5Sn//Li half-cell was lithiated to 0 V and delithiated to 1.5 V at 0.5 mA cm^{-2}. As shown in Figure S11 in the Supporting Information, the lithiation and delithiation specific capacities are 506 and 800 mAh g^{-1}, respectively, giving an initial Coulombic efficiency of 158%, which has been greatly improved, compared to that of 3Ag0.5Cu96.5Sn//Li (ICE = 10%). To examine the cycle performance, we perform galvanostatic lithiation at a constant capacity of 3 mAh cm^{-2} at 0.3C and then delithiated to 1.5 V at the same rate. As shown in Figure S12 in the Supporting Information, the initial Coulombic efficiency is up to 190%, indicating the
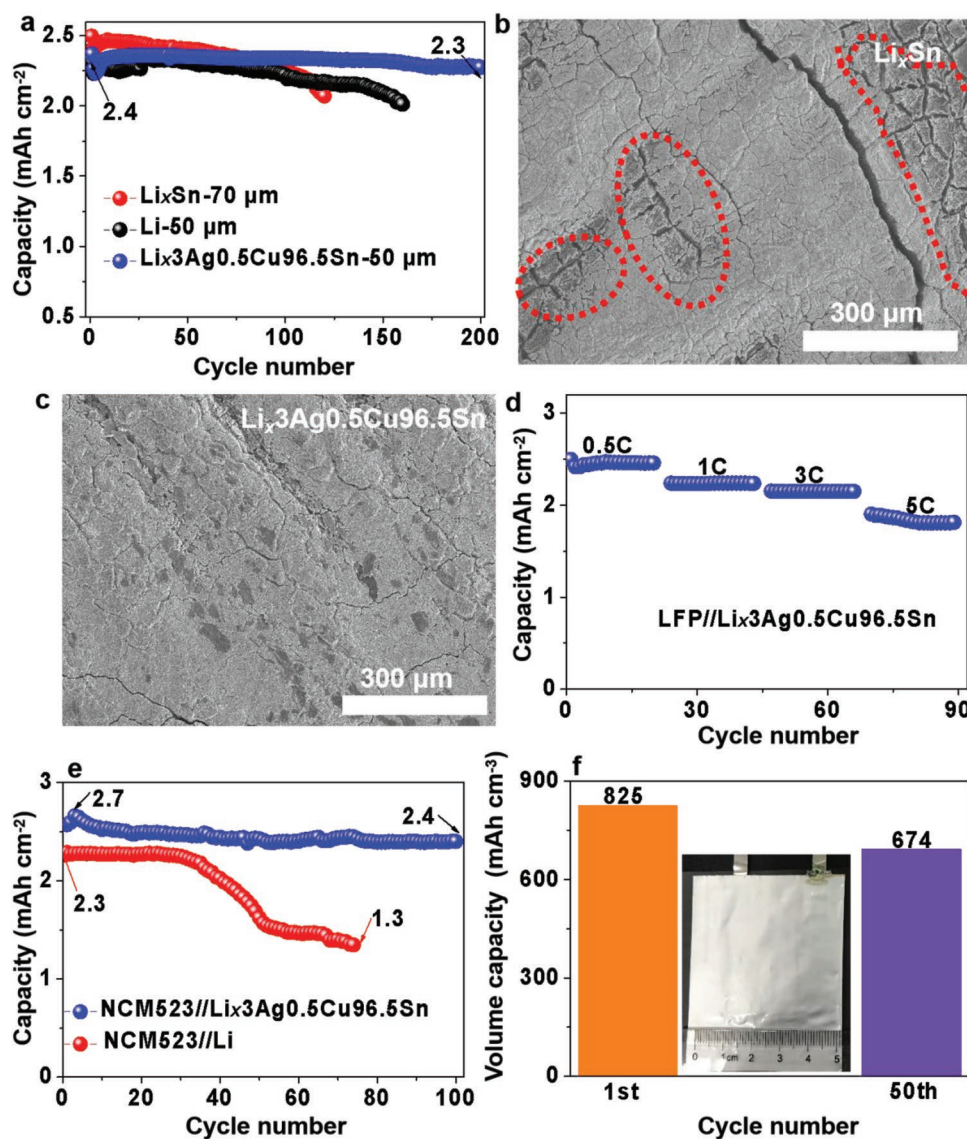
**ADVANCED
SCIENCE NEWS**

www.advancedsciencenews.com

**ADVANCED
ENERGY
MATERIALS**

www.advenergymat.de

Figure 7. Full cell performance and volume capacity density of $Li_x3Ag0.5Cu96.5Sn$ foil. a) Cycle performance of LFP//$Li_x3Ag0.5Cu96.5Sn$ and LFP//Li_xSn full cells. SEM characterization of b) the cycled Li_xSn and c) $Li_x3Ag0.5Cu96.5Sn$ foil electrodes and both of them have cycled 100 times in full cells against LFP cathode. d) Rate performance of LFP//$Li_x3Ag0.5Cu96.5Sn$ full cell. e) Cycle performance of NCM523//$Li_x3Ag0.5Cu96.5Sn$ full cell and NCM523//Li metal cell. f) Volume capacity density of $Li_x3Ag0.5Cu96.5Sn$ electrode in a pouch cell (3 cm × 2.8 cm).

prestored lithium is cyclable. Then second CE decreases to 95% due to lithium consumption that is originated from pulverization and electrolyte decomposition. Afterward, the CE gradually increases to 99.75% at fifth cycle and achieves an average CE of 99.82% (not considering the first cycle; the average CE would be 101.64% if the first cycle is included) in the first 50 cycles, implying the electrode maintains morphologically stable and parasitic reactions are constrained.

To compare electrochemical performance of Li_xSn and $Li_x3Ag0.5Cu96.5Sn$ foils with as little influence of cathode as possible, we chose the commercially available and very stable LFP cathode of ≈2.65 mAh cm^{-2} areal capacity in full-cell configuration. As shown in **Figure 7**a and Figure S13 in the Supporting Information, the as-prepared $Li_x3Ag0.5Cu96.5Sn$ alloy (the blue) achieves 95% capacity

retention in LFP//$Li_x3Ag0.5Cu96.5Sn$ full cell after 200 cycles at a current density of 0.4C. This level of performance is far superior to pure Li-metal foil of the same thickness in common LiPF$_6$-in-carbonates liquid electrolyte (see Figure 7a, the black). However, for 70 μm Li_xSn without the minor alloying elements (Figure 7a, the red), an obvious capacity decay could be observed after 80 cycles and the capacity retention was 82% after 120 cycles, after which the cell died rapidly. We dissembled cells after 100 cycles and found the large cracks on the Li_xSn surface in Figure 7b. Also, parts surrounded by the red dashed lines in Figure 7b were much less involved in electrochemical reactions compared to the other regions, indicative of lack of access to liquid electrolyte (due to electrolyte localization elsewhere[41]) and/or electronic failures (due to fracture, pulverization, and solid electrolyte interphase (SEI)

**ADVANCED
SCIENCE NEWS**

www.advancedsciencenews.com

**ADVANCED
ENERGY
MATERIALS**

www.advenergymat.de

insertion elsewhere). As shown in Figure S14 in the Supporting Information, Li_xSn foil that has cycled deeply 100 times is seriously pulverized, and can be likened to a garbage dump that is mixed with electrolyte decomposition products and inactivated Sn debris. In contrast, in $Li_x3Ag0.5Cu96.5Sn$ electrode that also deeply cycled 100 times, as shown in Figure 7c, the cracks on electrode surface (Figure 4b) were repaired, and a denser layer of SEI covered on the surface, which prevents continuous corrosion of electrode by the electrolyte, thus, the reaction depth keeps at ≈20 μm and the electrode is stable in Figure S15 in the Supporting Information. In addition to the striking improvement in cycle performance, the rate performance of $Li_x3Ag0.5Cu96.5Sn$ is attractive after the activation of initial cycles. As shown in Figure 7d, even at a rate of 5C, the discharge capacity density is still ≈1.8 mAh cm^{-2}. Furthermore, we paired $Li_x3Ag0.5Cu96.5Sn$ against NCM523 cathode of ≈3 mAh cm^{-2} areal capacity for higher full-cell voltage output (Figure 7e and Figure S16, Supporting Information). We found the cycle life of NCM523//$Li_x3Ag0.5Cu96.5Sn$ full cell (indicated with the blue) was twice of that of NCM523// Li metal foil cell (the red) pairing against equally thick Li foil anode of 50 μm. Thus, $Li_x3Ag0.5Cu96.5Sn$ seems a much more attractive option to work with than pure Li metal foil.[42]

In addition to the coin cell, we have also fabricated a 3 cm × 2.8 cm pouch cell to evaluate the cycling performance. Two commercial LFP cathodes were paired against one 70 μm thick $Li_x3Ag0.5Cu96.5Sn$ foil anode on both sides: in other words, the effective anode thickness against one cathode is only 35 μm, only about half of the thickness of commercial graphite anode at equal areal capacity of 2.65 mAh cm^{-2}. The initial discharge capacity of the pouch cell is ≈50 mAh (Figure S17, Supporting Information) and the corresponding initial volume capacity density is up to 825 mAh cm^{-3} (Figure 7f, the orange bar). As shown in Figure S17 in the Supporting Information, the pouch cell shows quite stable cycle performance after 50 cycles. Subsequently, the pouch cell was disassembled and the anode electrode thickness was measured to estimate the actual capacity density after cycling. The thickness increased to ≈87 μm from the initial 70 μm, a surprisingly small amount of expansion for such high capacity anode. The volumetric capacity of $Li_x3Ag0.5Cu96.5Sn$ foil was still up to 674 mAh cm^{-3} (Figure 7f, the purple). The surface of cycled $Li_x3Ag0.5Cu96.5Sn$ foil from pouch cell also was observed by SEM, as shown in Figure S18 in the Supporting Information, a layer of dense SEI film protects $Li_x3Ag0.5Cu96.5Sn$ electrode from continuous corrosion and pulverization.

3. Conclusion

In this study, a mechanical prelithiation and rolling down approach based on 3Ag0.5Cu96.5Sn alloy foil is developed to prepare a thin free-standing and Li-containing foil anode. It is found the grain size refinement by doping Ag and Cu elements is an effective strategy to reduce electrode damage because of more grain boundary sliding systems to release residual stress of prelithiation process, and thus thinner prelithiated foil electrode can be achieved for higher capacity density. Also, due to

Li^+(electrolyte) transport in the liquid electrolyte along the GB replacing the Li(metallic) transport along GB after prelithiation, Li^+ diffusion of $Li_x3Ag0.5Cu96.5Sn$ is increased by an order of magnitude and the Faraday impedance decreased to 75 Ω from 1500 Ω. Besides, due to Li-Sn-O(H) products in situ formed on surface when contacting open air, $Li_x3Ag0.5Cu96.5Sn$ foil has excellent air stability and the capacity retention is 90% after exposed to air for 48 h. The full cells paring the as-prepared 50 μm $Li_x3Ag0.5Cu96.5Sn$ foil against both commercial LFP and NCM523 cathodes exhibit excellent battery performance. Additionally, the practical value was demonstrated in a LFP// $Li_x3Ag0.5Cu96.5Sn$ pouch cell, which displayed a volume capacity density of 825 mAh cm^{-3} at first cycle and the capacity density retention is ≈82% after 50th cycle. This work overcomes the major limitations associated with anode materials of low ICE and open new avenues for developing free-standing foil-like electrodes with high capacity density.

4. Experimental Section

Materials: 3Ag0.5Cu96.5Sn and pure Sn foils (40–100 μm, Zhenjiang Fan Yada Electronic Technology Co., Ltd.) were punched into discs with a diameter of 12 mm and then directly used as working electrodes. The mechanical prelithiation was carried out as follows: Li foil (China Energy Lithium Co., Ltd.) and Sn foil (40–100 μm) were stacked together and pressed with a roller (MSK-2150, Shenzhen Kejing Star Technology, Ltd.) at 30 MPa pressure. Since Li foil (50 μm) is used both sides, for the sake of simplicity, the roll-to-roll approach was simplified into "a 45 μm × 10 cm × 3.5 cm 3Ag0.5Cu96.5Sn foil and a 25 μm × 10 cm × 3.5 cm Li foil were stacked." The as-prepared prelithiated foil was punched into discs or designed dimensions of pouch cell and then directly used as electrodes. The commercial LFP (active material is 18.97 mg cm^{-2}) and NCM523 (active material is 12 mg cm^{-2}) cathodes with an area capacity density of ≈3 mAh cm^{-2} were purchased from MTI.

Characterization: Grain size and microstructure of foils were observed via optical microscopy (6XB-PC, Optical instrument factory) and TEM (TF20, JOEL 2100F). The solution that consists of 1.5 vol% HCl, 1 vol% HNO₃, and 97.5 vol% methanol was employed to corrode foils for grain observation. The surface and cross-section morphology was observed via a field emission SEM (FEI Quanta 200). The phase structure of foil was identified by XRD (Bruker AXS GMBH GERM D8) with CuK$_\alpha$ radiation (λ = 1.54184 Å). The signal was collected for diffraction angles (2θ) between 10° and 80° at a scan rate of 3° min^{-1}, Kapton tape was used to protect the lithiated foil from air contamination. The contact angle between electrode surface and electrolyte was examined by a contact angle meter (JC2000D1, Shanghai Zhongchen Digital Technology Equipment Co., Ltd.).

Electrochemical Measurements: The electrochemical measurement was measured in CR2025 coin-type cell using a test system (CT-4008, Neware). The separator was Celgard 2400 and the electrolyte of Sn//Li half-cell and LFP//Li_xSn, LFP//$Li_x3Ag0.5Cu96.5Sn$ was 1 M LiPF₆ solved in EC/DEC (v/v = 1:1) with 10% FEC and 1% VC as additives, and the electrolyte of NCM523// $Li_x3Ag0.5Cu96.5Sn$ and NCM523//Li cells was purchased from Hubei Jiubang New Energy Technology Co., Ltd. (NP6054A1). The Sn//Li half-cell was lithiated to 3 mAh and then delithiated to 1.5 V at 0.3C. CV and electrochemical impedance spectroscopy (EIS) measurements were performed on an electrochemical work station (CHI660E, Shanghai Chen Hua Instrument Co., Ltd.). Specifically, CV test was successively carried out from 0 to 1.5 V at scan rates of 0.02, 0.05, 0.1, 0.2, and 0.5 mV s^{-1}. EIS test was performed from 10⁶ to 0.1 Hz. LFP//Li_xSn and LFP//$Li_x3Ag0.5Cu96.5Sn$ full cells were charged to 3.8 V and then discharged to 2 V at 0.4C. NCM523//$Li_x3Ag0.5Cu96.5Sn$ full cell was charged to 4.3 V and then discharged to 2.8 V at 0.4C.

Supporting Information

Acknowledgements

Conflict of Interest

The authors declare no conflict of interest.

Keywords

[1] S. Han, B. Jang, T. Kim, S. M. Oh, T. Hyeon, *Adv. Funct. Mater.* **2005**, *15*, 1845.

[2] D. H. Youn, S. K. Stauffer, P. Xiao, H. Park, Y. Nam, A. Dolocan, G. Henkelman, A. Heller, C. B. Mullins, *ACS Nano* **2016**, *10*, 10778.

[3] S. Yang, P. Y. Zavalij, M. S. Whittingham, *Electrochem. Commun.* **2003**, *5*, 587.

[4] Y. Jin, S. Li, A. Kushima, X. Zheng, Y. Sun, J. Xie, J. Sun, W. Xue, G. Zhou, J. Wu, F. Shi, R. Zhang, Z. Zhu, K. So, Y. Cui, J. Li, *Energy Environ. Sci.* **2017**, *10*, 580.

[5] S. Zhang, Y. Xing, T. Jiang, Z. Du, F. Li, L. He, W. Liu, *J. Power Sources* **2011**, *196*, 6915.

[6] X. Zhou, J. Bao, Z. Dai, Y.-G. Guo, *J. Phys. Chem. C* **2013**, *117*, 25367.

[7] R. Z. Hu, Y. Zhang, M. Zhu, *Electrochim. Acta* **2008**, *53*, 3377.

[8] A. Veluchamy, C.-H. Doh, D.-H. Kim, J.-H. Lee, D.-J. Lee, K.-H. Ha, H.-M. Shin, B.-S. Jin, H.-S. Kim, S.-I. Moon, C.-W. Park, *J. Power Sources* **2009**, *188*, 574.

[9] L. Yang, L.-Y. Sun, R.-R. Zhang, Y.-W. Xu, X.-H. Ning, Y.-B. Qin, R. L. Narayan, J. Li, Z.-W. Shan, *J. Mater. Chem. A* **2018**, *6*, 15738.

[10] Y.-L. Kim, S.-J. Lee, H.-K. Baik, S.-M. Lee, *J. Power Sources* **2003**, *119–121*, 106.

[11] N. Tamura, R. Ohshita, M. Fujimoto, S. Fujitani, M. Kamino, I. Yonezu, *J. Power Sources* **2002**, *107*, 48.

[12] H. Xu, S. Li, C. Zhang, C. X. Long, L. W. Jian, X. Yong, Y. Zheng, Y. Huang, J. Li, *Energy Environ. Sci.* **2019**, https://doi.org/10.1039/C9EE01404G.

[13] H. J. Kim, S. Choi, S. J. Lee, M. W. Seo, J. G. Lee, E. Deniz, Y. J. Lee, E. K. Kim, J. W. Choi, *Nano Lett.* **2016**, *16*, 282.

[14] T. Tabuchi, H. Yasuda, M. Yamachi, *J. Power Sources* **2005**, *146*, 507.

[15] T. Tabuchi, H. Yasuda, M. Yamachi, *J. Power Sources* **2006**, *162*, 813.

[16] H. Takezawa, S. Ito, H. Yoshizawa, T. Abe, *Chem. Lett.* **2017**, *46*, 1365.

[17] J. Zhao, J. Sun, A. Pei, G. Zhou, K. Yan, Y. Liu, D. Lin, Y. Cui, *Energy Storage Mater.* **2018**, *10*, 275.

[18] C. Herring, *J. Appl. Phys.* **1950**, *21*, 437.

[19] S. Zhang, K. Zhao, T. Zhu, J. Li, *Prog. Mater. Sci.* **2017**, *89*, 479.

[20] A. Zhu, D. Zhang, T. Zhu, Y. Guo, *Sci. China: Earth Sci.* **2018**, *61*, 1644.

[21] Q. Wang, P. Zhang, Z. Niu, J. T. Freymueller, X. A. Lai, Y. Li, W. Zhu, J. Liu, R. Bilham, K. M. Larson, *Sci. China, Ser. D: Earth Sci.* **2002**, *45*, 865.

[22] G. Derrien, J. Hassoun, S. Panero, B. Scrosati, *Adv. Mater.* **2007**, *19*, 2336.

[23] J. W. Cahn, *Acta Metall.* **1956**, *4*, 449.

[24] R. Raj, M. F. Ashby, *Metall. Trans.* **1971**, *2*, 1113.

[25] T. G. Langdon, *J. Mater. Sci.* **2006**, *41*, 597.

[26] T. G. Langdon, *Philos. Mag.* **1970**, *22*, 689.

[27] M. O. Alam, Y. C. Chan, K. N. Tu, *Chem. Mater.* **2003**, *15*, 4340.

[28] J. Görlich, G. Schmitz, K. N. Tu, *Appl. Phys. Lett.* **2005**, *86*, 053106.

[29] D. A. Shnawah, M. F. M. Sabri, I. A. Badruddin, *Microelectron. Reliab.* **2012**, *52*, 90.

[30] S. Cheng, C.-M. Huang, M. Pecht, *Microelectron. Reliab.* **2017**, *75*, 77.

[31] G. Zeng, S. Xue, L. Zhang, L. Gao, W. Dai, J. Luo, *J. Mater. Sci.: Mater. Electron.* **2010**, *21*, 421.

[32] J. Glazer, *J. Electron. Mater.* **1994**, *23*, 693.

[33] X. Ma, F. Wang, Y. Qian, F. Yoshida, *Mater. Lett.* **2003**, *57*, 3361.

[34] Z. Nishiyama, H. Morikawa, K. i. Shimizu, *Jpn. J. Appl. Phys.* **1967**, *6*, 815.

[35] K. S. Kim, S. H. Huh, K. Suganuma, *Mater. Sci. Eng., A* **2002**, *333*, 106.

[36] C.-M. Chuang, P.-C. Shih, K.-L. Lin, *J. Electron. Mater.* **2004**, *33*, 1.

[37] M. W. Jingtian Yin, S. Yoshida, K. Ishihara, S. Tanase, a. T. Sakai, *J. Electrochem. Soc.* **2003**, *1507*.

[38] S. Han, J. Park, W. Lu, A. M. Sastry, *J. Power Sources* **2013**, *240*, 155.

[39] J. Tian, Y. Su, F. Wu, S. Xu, F. Chen, R. Chen, Q. Li, J. Li, F. Sun, S. Chen, *ACS Appl. Mater. Interfaces* **2016**, *8*, 582.

[40] H.-B. Sun, Y.-X. Zhou, L.-L. Zhang, X.-L. Yang, X.-Z. Cao, H. Arave, H. Fang, G. Liang, *Phys. Chem. Chem. Phys.* **2017**, *19*, 5155.

[41] M. Jiang, Y. Yu, H. Fan, H. Xu, Y. Zheng, Y. Huang, S. Li, J. Li, *ACS Appl. Mater. Interfaces* **2019**, *11*, 15656.

[42] S. Li, M. Jiang, Y. Xie, H. Xu, J. Jia, J. Li, *Adv. Mater.* **2018**, *30*, 1706375.

**ADVANCED
ENERGY
MATERIALS**

Supporting Information

Sn-Alloy Foil Electrode with Mechanical Prelithiation: Full-Cell Performance up to 200 Cycles

Hui Xu, Sa Li,* Xinlong Chen, Can Zhang, Wenjian Liu, Huimin Fan, Yue Yu, Yunhui Huang,* and Ju Li*

Supporting Information

Sn-alloy foil electrode with mechanical prelithiation: full-cell performance up to 200 cycles

Hui Xu[1,2†], Sa Li[1,2*†], Xinlong Chen[1,2], Can Zhang[1,2], Wenjian Liu[1,2], Huimin Fan[1,2], Yue Yu[1,2], Yunhui Huang[1,2*] and Ju Li[3*]

[1]School of Materials Science and Engineering, Tongji University, Shanghai 201804, China
[2]Institute of New Energy for Vehicles, Tongji University, Shanghai 201804, China
[3]Department of Nuclear Science and Engineering and Department of Materials Science and Engineering, Massachusetts Institute of Technology, Cambridge, MA 02139, USA
[†]These authors contributed equally to this work
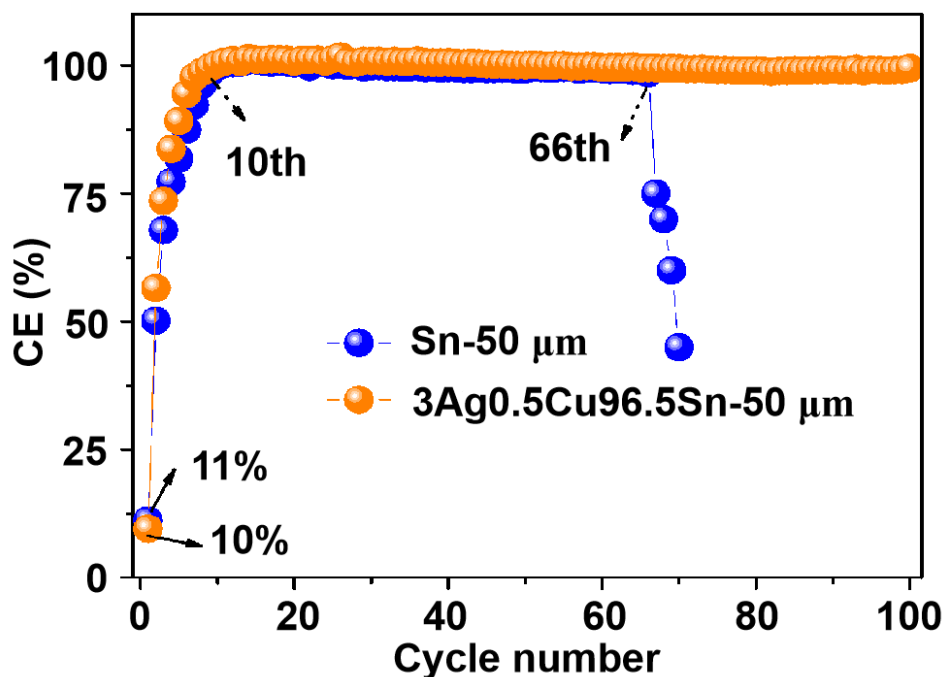
Figure S1. Coulombic efficiency (CE) analysis of Sn based foil electrodes. Sn//Li and 3Ag0.5Cu96.5Sn//Li half cells were lithiated to 3 mAh cm^{-2} and then delithiated to 1.5 V. The initial Coulombic efficiency (ICE) of both foils is only ~ 10%. However, cells can keep stably more than 100 cycles after the first cycles, implying Sn based foil electrode may be a potential anode for LIBs after improving ICE.
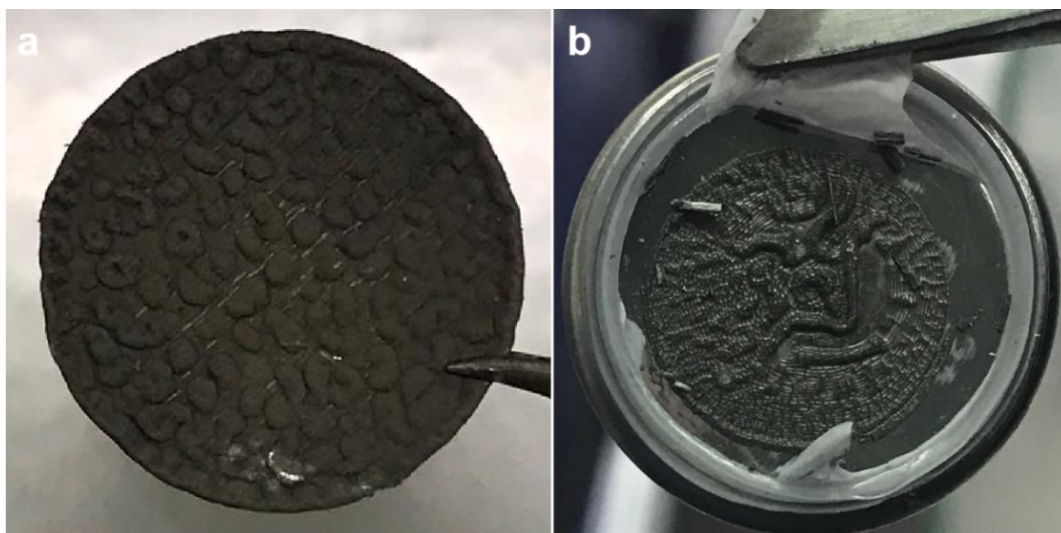
Figure S2. Digital photos of Sn foil that was prelithiated by the electrochemical method. a,b) There are visual millimeter-scale mountain range-like undulations after electrochemical lithiation.
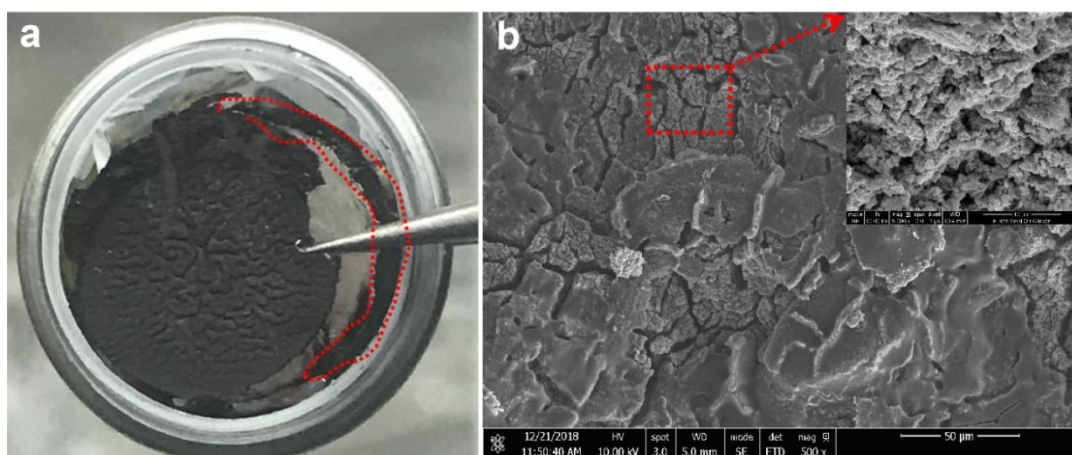
Figure S3. Digital photos of cycled Sn foil electrodes. a) The optical photo of cycled Sn foil. The black material scattered around the coin cell is shedding Sn debris. b) SEM image of the cycled Sn foil surface.
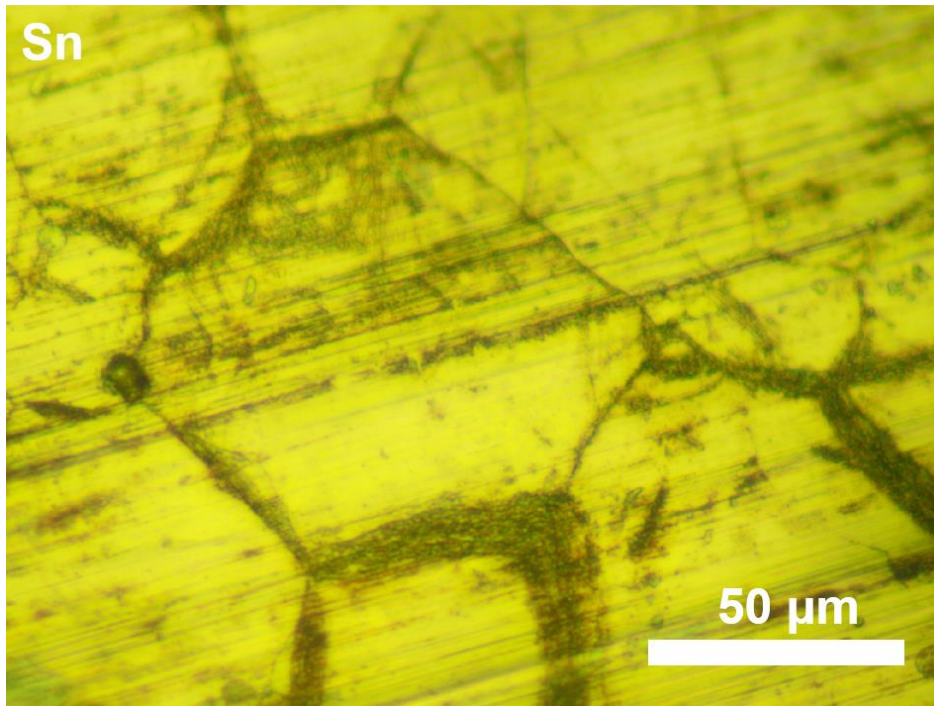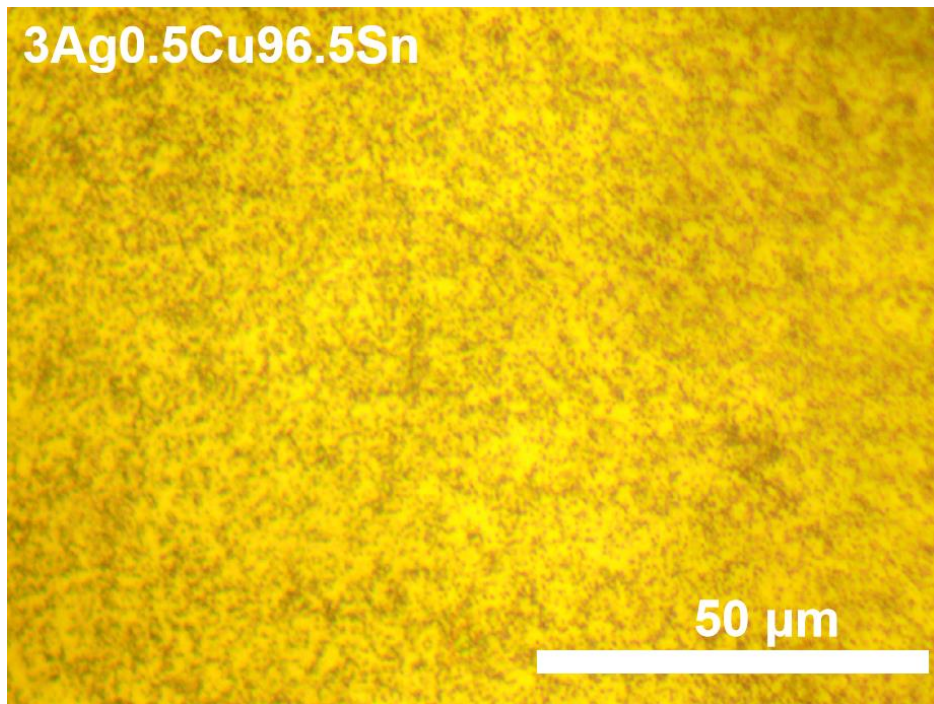
Figure S4. Grain observation of Sn foil was performed by an optical microscope.

Figure S5. The optical observation of etched 3Ag0.5Cu96.5Sn foil was carried out by an optical microscope. The grain of 3Ag0.5Cu96.5Sn was so small that optical microscope cannot clearly identify it.
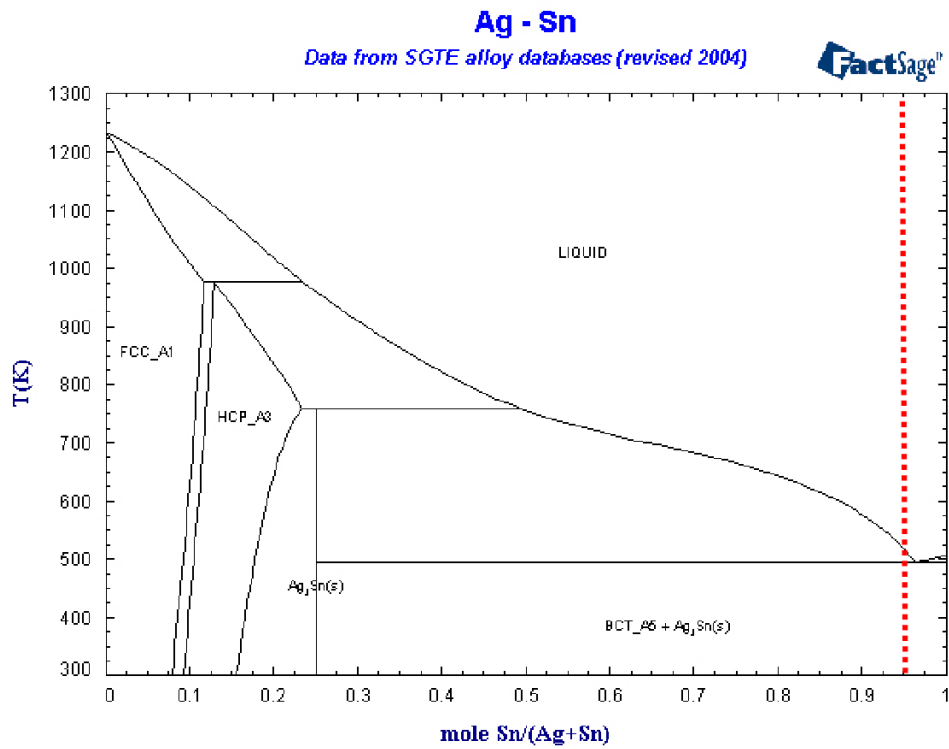
Figure S6. Ag-Sn binary phase diagram.
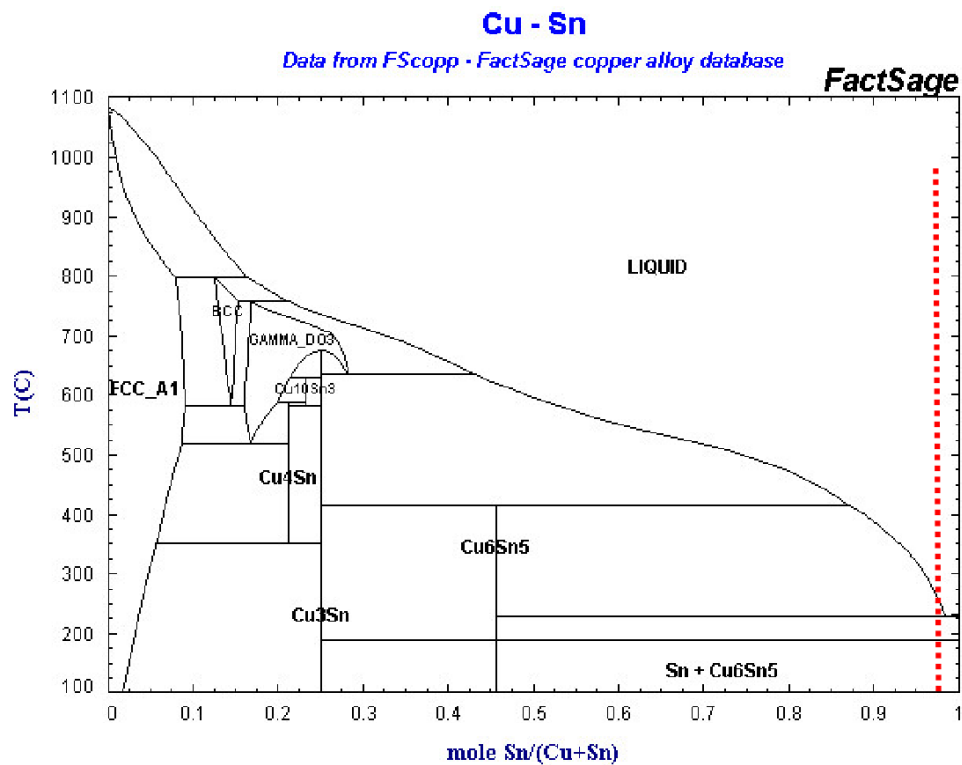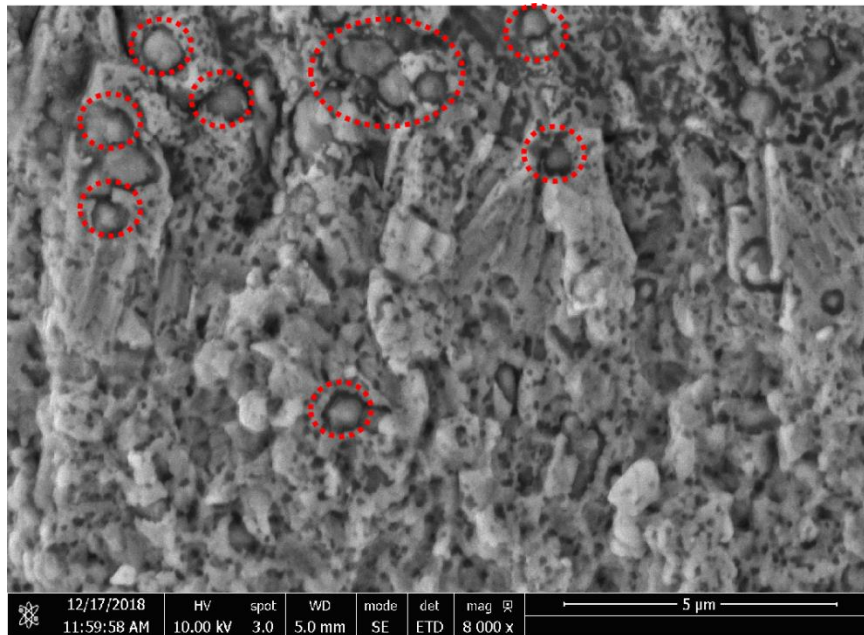

Figure S7. Cu-Sn binary phase diagram.

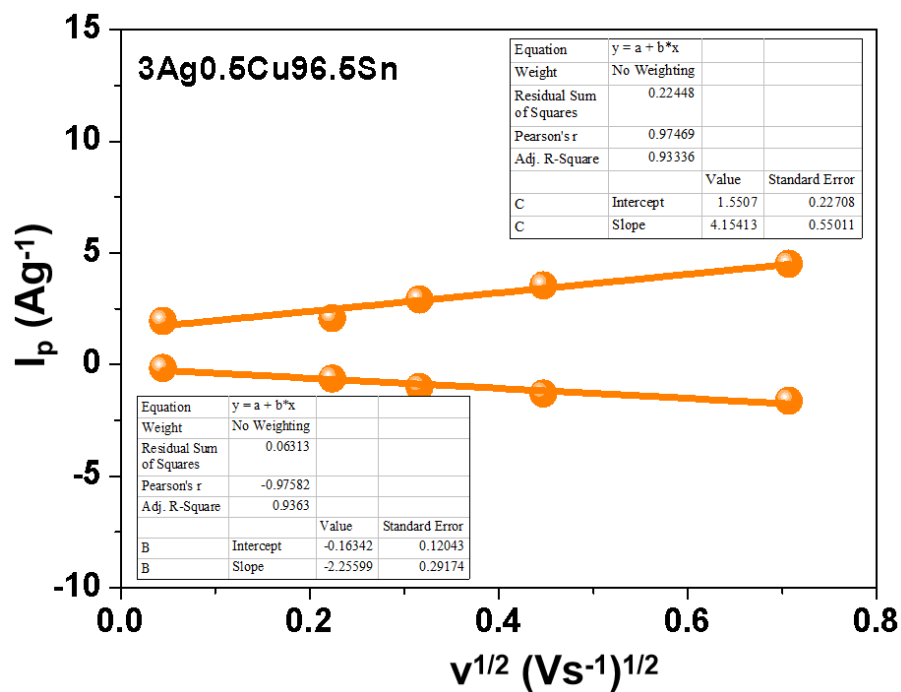**Figure S8.** Nano Ag$_3$Sn particles embedded in the matrix were determined by SEM.

3Ag0.5Cu96.5Sn

Equation	y = a + b*x	
Weight	No Weighting	
Residual Sum of Squares	0.22448	
Pearson's r	0.97469	
Adj. R-Square	0.93336	
	Value	Standard Error
C Intercept	1.5507	0.22708
C Slope	4.15413	0.55011

Equation	y = a + b*x	
Weight	No Weighting	
Residual Sum of Squares	0.06313	
Pearson's r	-0.97582	
Adj. R-Square	0.9363	
	Value	Standard Error
B Intercept	-0.16342	0.12043
B Slope	-2.25599	0.29174

Figure S9. The fitting result of linear relationship between peak current and square root of scan rate of 3Ag0.5Cu96.5Sn.
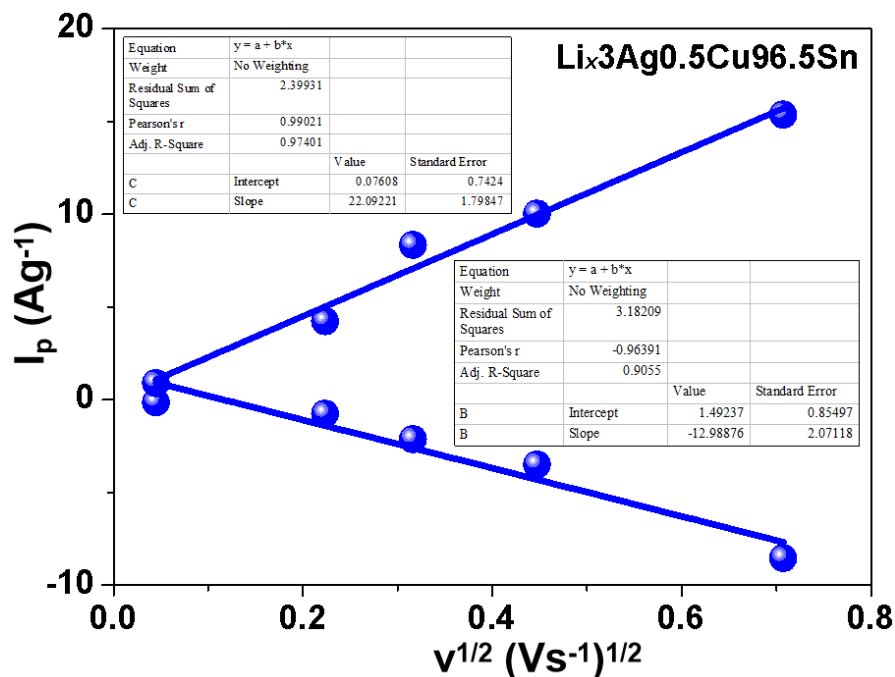
Figure S10. The fitting result of linear relationship between peak current and square root of scan rate of Li$_x$3Ag0.5Cu96.5Sn.
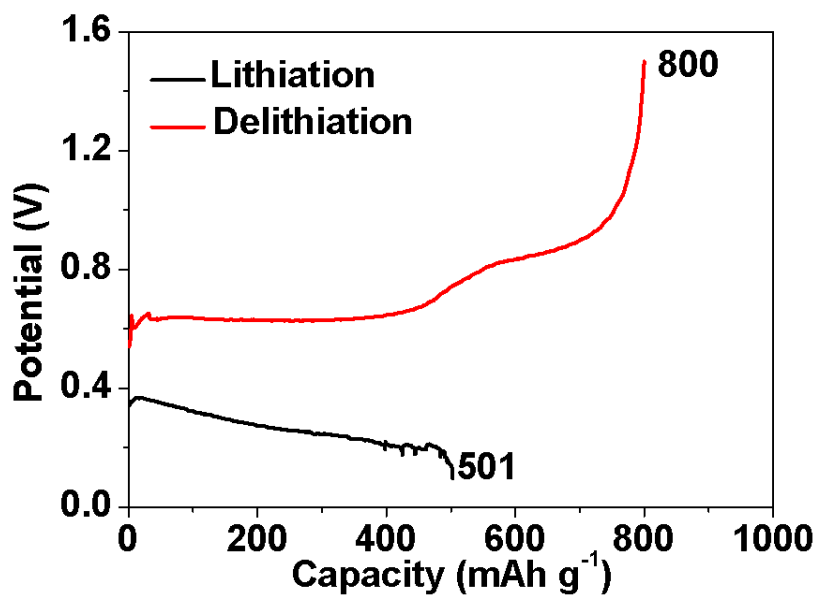

Figure S11. Capacity-potential curves of Li$_x$3Ag0.5Cu96.5Sn//Li half-cell. In order to determine the specific capacity of Li$_x$3Ag0.5Cu96.5Sn electrode, a disc with a diameter of 8 mm (11.68 mg in weight) was paired against lithium metal. The Li$_x$3Ag0.5Cu96.5Sn//Li half-cell was lithiated to 0 V and delithiated to 1.5 V at 0.5 mA cm^{-2}. The lithiation and delithiation specific capacities are 506 mAh g^{-1} and 800 mAh g^{-1}, respectively, giving an initial Coulombic efficiency of 158 %, which has been greatly improved, compared to that of 3Ag0.5Cu96.5Sn//Li (CE=10%).
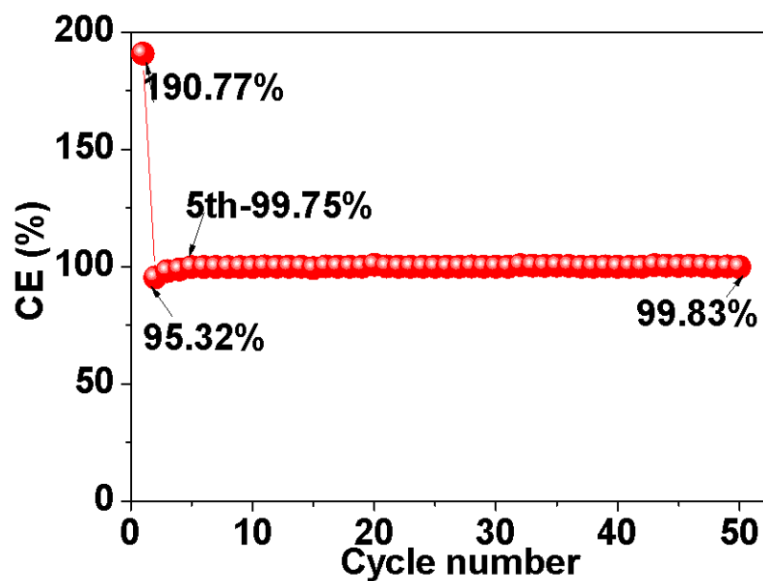
Figure S12. Coulombic efficiency (CE) analysis of Li$_x$3Ag0.5Cu96.5Sn foil anode. To examine the cycle performance, we performed galvanostatic lithiation at a constant capacity of 3 mAh cm^{-2} at 0.3 C and then delithiated to 1.5 V at the same rate. The initial Coulombic efficiency is up to 190%, indicating the pre-stored lithium is cyclable. Then second CE decreases to 95% due to lithium consumption that is originated from pulverization and electrolyte decomposition. Afterwards, the CE gradually increases to 99.75% at 5th cycle and achieves an average CE of 99.82% (not consider the first cycle, and average CE would be 101.64% if the first cycle is included) in the first 50 cycles, implying the electrode might maintain morphologically stable and parasitic reactions are constrained.
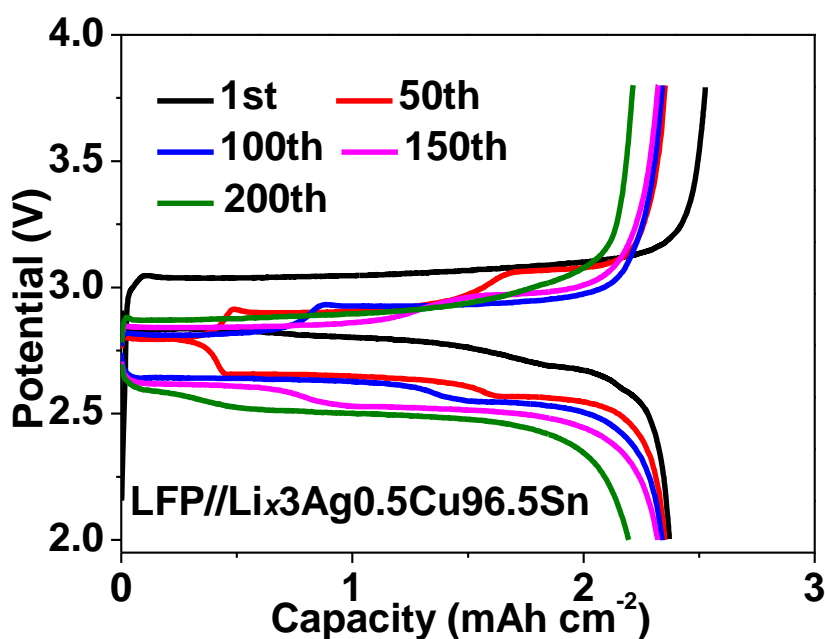
Figure S13. Charge-discharge curves of LFP//Li$_x$3Ag0.5Cu96.5Sn full cell. The cell was cycled at 0.4 C based on LFP cathode.

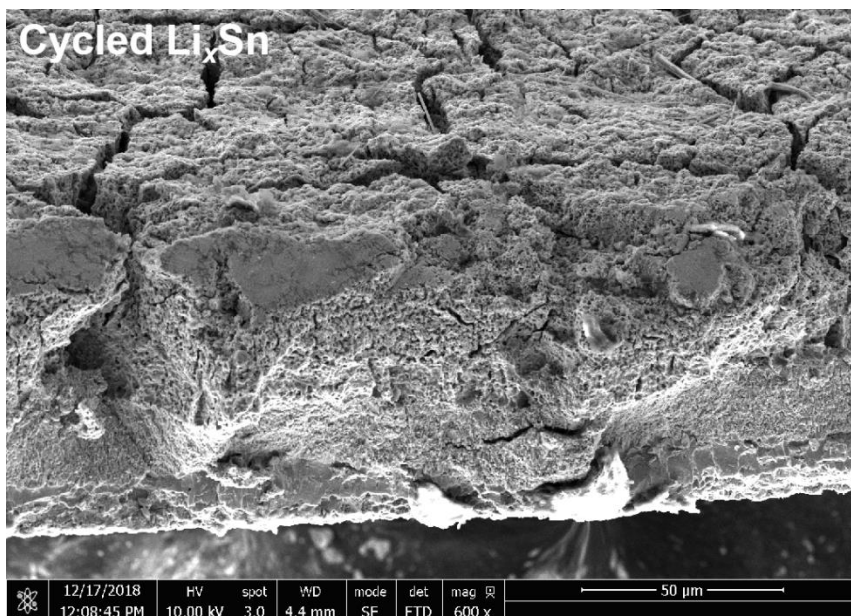**Figure S14.** Cross-sectional SEM of cycled Li$_x$Sn foil after 100 cycles.
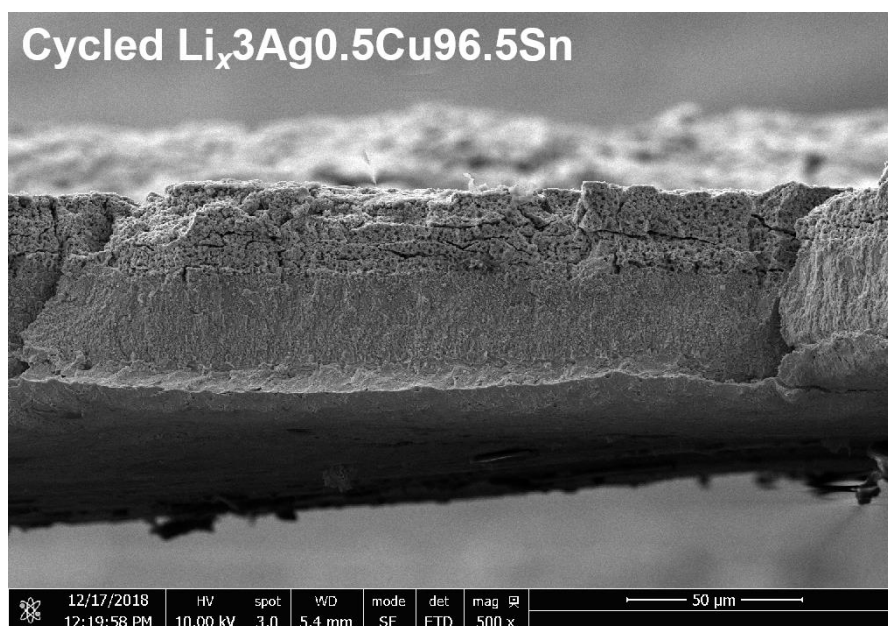

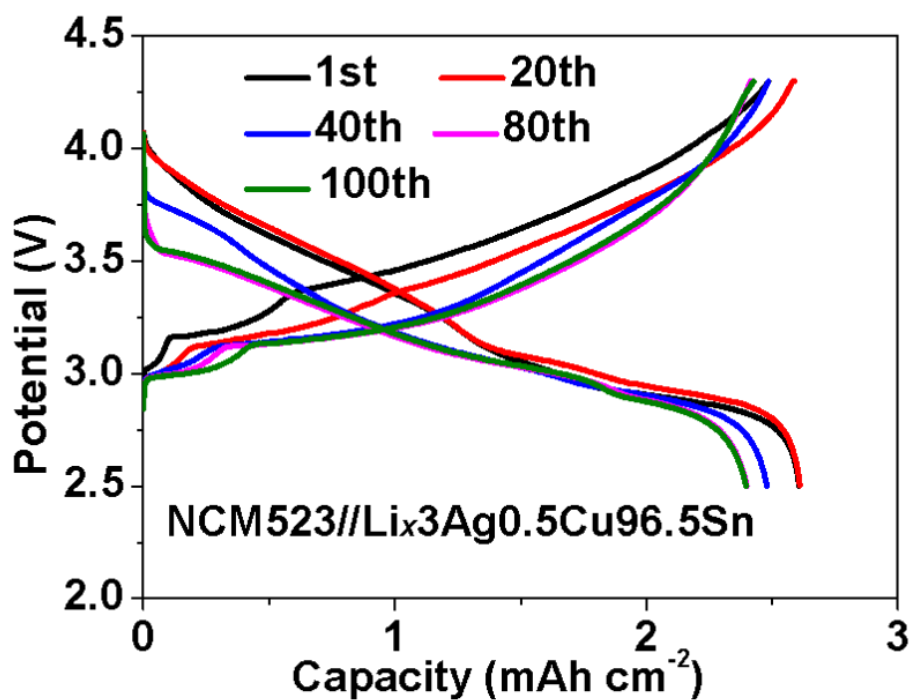**Figure S15.** Cross-sectional characterization of cycled Li$_x$3Ag0.5Cu96.5Sn foil after 100 cycles.

Figure S16. Charge-discharge curves of NCM523//Li$_x$3Ag0.5Cu96.5Sn full cell. The cell was cycled at 0.4 C based on NCM523 cathode.
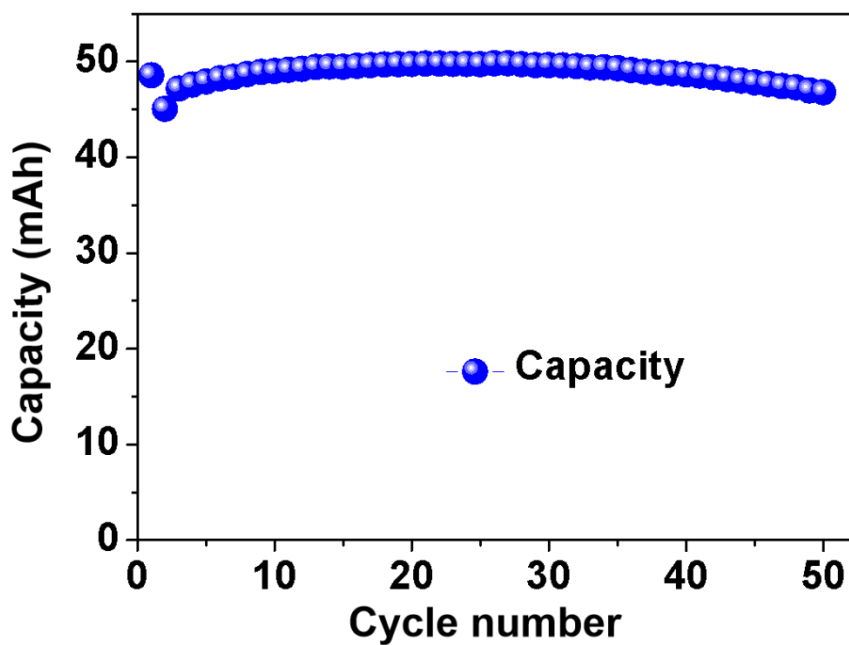

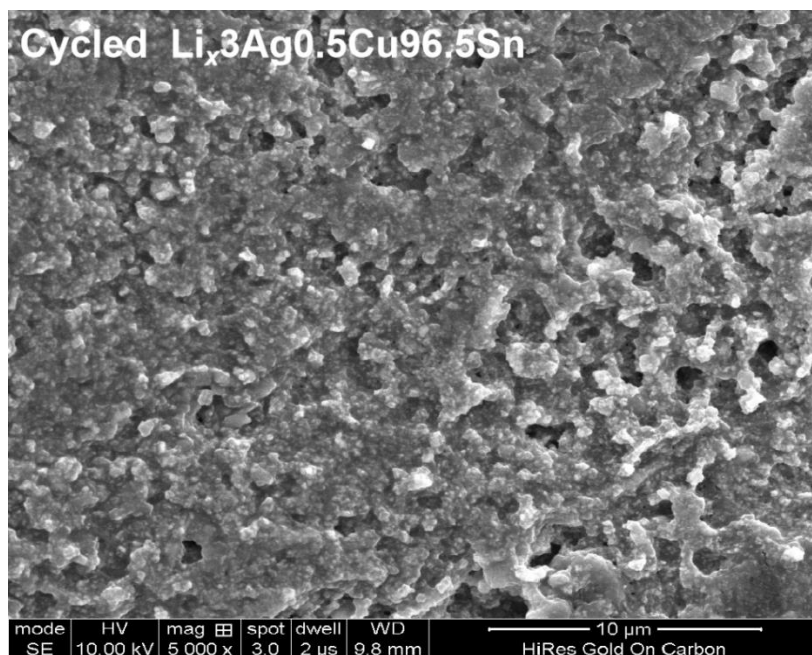**Figure S17.** Discharge capacity of LFP//Li$_x$3Ag0.5Cu96.5Sn pouch cell.

Figure S18. Surface characterization of cycled Li$_x$3Ag0.5Cu96.5Sn foil electrode of pouch cell. The dense SEI layer covered on the Li$_x$3Ag0.5Cu96.5Sn foil surface effectively hinders continuous corrosion of the electrode by the electrolyte.